EFFECT OF BLADE NUMBER ON OPTIMUM ROTOR PERFORMANCE IN AXIAL FLOW WITH SWIRL

Chad L. File

Graduate Research Assistant

cfile@wustl.edu

Ramin Modarres

Graduate Research Assistant

ramin.modarres@wustl.edu

David A. Peters

McDonnell Douglas Professor of Engineering

dap@wustl.edu

Department of Mechanical Engineering & Materials Science

Washington University in Saint Louis

Saint Louis, Missouri 63130

July 10, 2012

Abstract

Dynamic inflow theory is used to develop an analytical formulation for the general performance of the lifting rotor in axial flow with finite blade number and improved swirl correction. The theory incorporates conventional blade-element theory for blade lift and provides the integrated loads and the induced power of the rotor in terms of an arbitrary number of blades. A finite-state model of the rotor provides the basis for a classical quadratic optimization with realistic constraints that is applied to determine the minimum induced power for a variety of available control combinations, rotor trim constraints, number of blades, and operating conditions. The findings show relative agreement to the classical propeller solutions predicted by Golstein at moderate to high inflow ratios. Swirl vortices—due to finite number of blades—significantly reduce the non-ideal induced power increment. New insights are given for some of the factors that prevent practical rotors from achieving Golstein's predicted efficiency. Improvements to the swirl correction give greater understanding to the nature of this puzzling phenomenon. Limited comparisons with previous research corroborate the earlier results and demonstrate the versatility of the present formulation.

Notation

a	slope of the lift curve, (rad^{-1})
a_n^m	induced flow states (Peters-He model)
aoa	angle of attack
$[A]$	transformation matrix
c	chord length
c_l	roll moment per thrust, C_L/C_T
c_m	pitch moment per thrust, C_M/C_T
C_L	roll moment coefficient
$C_{\mathscr{L}}$	lift coefficient
C_M	pitch moment coefficient
C_T	thrust coefficient
$\{C\}$	rotor loads and loading constraints
$[C]$	temporal transformation matrix
$[D]$	loads matrix
$[E]$	orthogonality matrix
$[G]$	matrix of loading constraints
$[I]$	identity matrix
k	integer multiple of number of blades
K	number of control radial functions
$\mathscr{L}$	blade lift per unit length
$[\tilde{L}]$	influence coefficient matrix (Peters-He model)
$[\bar{L}]$	influence coefficient matrix
$[\bar{\bar{L}}]$	coupled mass and influence coefficient matrix
M	number of control harmonics
$[M]$	apparent mass matrix (Peters-He model)
$[M]_{\texttt{swirl}}$	modified apparent mass matrix
$[N]$	decoupling transformation matrix
$\bar{P}_n^m()$	normalized associated Legendre function
ΔP	pressure drop across the disk
Q	total number of blades
$[Q]$	symmetric optimizing matrix
$\bar{r}$	non-dimensional radial position
R	rotor radius
$[R]$	harmonic expansion of coupling matrix
t	time, (s)
$\bar{t}$	non-dimensional reduced time, (Ωt)
$[T]$	harmonic transformation matrix
U_P	perpendicular component of velocity
U_T	tangential component of velocity

V	non-dimensional mass flow parameter
w	non-dimensional induced flow distribution
α_n^m, β_n^m	induced flow states
γ_n^m	lift expansion coefficients
$\delta_{n,n'}$	Kronecker delta function
ε_{IP}	induced-power efficiency
$\{\zeta\}$	vector of scaled loads
κ	empirical swirl factor
λ	inflow ratio
(ν, η, ξ)	ellipsoidal coordinates
ϱ	fluid density
τ_n^m	pressure expansion coefficients
χ	inflow skew angle
ψ	azimuth angle of blade from rotor aft
Ω	rotor rotational speed, (rad/s)
Subscript	
c, s	cosine or sine expansion in time
k	blade harmonic number
n, j	polynomial number
q	q^{th} blade
Superscript	
c, s	cosine or sine expansion in space
m, r	harmonic number

1. INTRODUCTION

The classical solutions by Goldstein give the effect of a finite number of blades on the optimum circulation distribution for a rotor in axial flow[1]. However, due to the complexity of the solution, results are given only for a 2-bladed rotor at several inflow ratios and a 4-bladed rotor at a single inflow ratio. Recently, finite-state inflow methods have shown that they have the capability to find the optimum circulation distribution for rotors by classical, quadratic optimization in closed form[2,3].

These methods can be applied to a helicopter in hover or in forward flight. For this, the closed-form results of Goldstein offer the perfect data set against which to check the convergence of the finite-state method; but the scarcity of cases by Goldstein has made this difficult. In recent work, we have been able to extend the Goldstein solutions to a wider variety of cases, and this now allows a complete verification of the finite-state convergence in axial flow[4].

In this paper, we study the convergence of the finite-state method—including the effect of wake swirl—to demonstrate the most efficient form of the swirl correction and to show that convergence is excellent with this method. New results are given that not only demonstrate the convergence but also illustrate the nature of the effect of blade number on the optimum performance. All of this is done under the framework of classical, quadratic optimization with the finite-state model.

2. AERODYNAMIC THEORY

2.1. Finite-State Inflow Model

The Finite-State Inflow Theory of Peters & He[5,6] has become an established foundation to model the dynamic inflow of the lifting rotor. In this theory, both the induced velocity and the pressure distribution is expanded in harmonics of Legendre functions. This expansion permits the fundamental laws of fluid flow to be restructered in matrix form. This has the advantage of greater computability and allows for the use of extensive numerical techniques.

In this model, the non-dimensional induced flow distribution is represented as the following.

$$(1) \qquad w = \sum_{m,n} \left[\alpha_n^m \cos(m\psi) + \beta_n^m \sin(m\psi) \right] \frac{\bar{P}_n^m}{\nu}$$

where $\bar{P}_n^m = \bar{P}_n^m(\nu)$ are normalized associated Legendre functions of the first kind.

$$(2) \qquad \bar{P}_n^m \equiv \frac{(-1)^m}{\rho_n^m} P_n^m$$

where the parameters ρ_n^m are the normalization functions defined by the following:

$$(3) \quad \int_0^1 P_n^m(x) P_{n'}^m(x) dx = \frac{(n+m)!}{(n-m)!} \frac{\delta_{n,n'}}{2n+1} \equiv (\rho_n^m)^2$$

The parameter ν is the ellipsoidal coordinate which, on the rotor disk ($\eta \equiv 0$), is given by

$$(4) \qquad \nu = \sqrt{1 - \bar{r}^2}$$

The subscripts and superscripts follow the notation presented in the Peters-He model where the superscript m is the harmonic number and the subscript n is a radial expansion number for a given harmonic. Note that Legendre functions are only defined for $n \geq m$.

Due to the definition of the ellipsoidal coordinate ν, which represents hyperbolas of revolution, any solution to Laplace's equation that are odd in ν represent a differential pressure across the disk. Therefore, as was the induced flow, the non-dimensional pressure across the rotor disk is also expanded in Legendre functions.

$$(5) \quad \Delta P = 2 \left[\sum_{m,n} \left[\tau_n^{mc} \cos(m\psi) + \tau_n^{ms} \sin(m\psi) \right] \bar{P}_n^m \right]$$

where the superscripts c and s represent cosine and sine expansions about the azimuth ψ.

Both the inflow states, α and β, and the pressure expansion coefficients, τ^c and τ^s, are expanded in temporal harmonics and, thus, time dependent. For example,

$$(6) \quad \alpha_n^m = \alpha_{n0c}^m + \sum_{k=Q_i} \left(\alpha_{nkc}^m \cdot \cos(kt) + \alpha_{nks}^m \cdot \sin(kt) \right)$$

where k takes on integer multiples of the number of blades (i.e., $k = Q_i = Q, 2Q, 3Q, ...$). Here the subscripts c and s represent cosine and sine expansions in time. Also, the zero harmonic terms $(\alpha_n^0(t))$ are defined in the following manner.

$$(7) \qquad \alpha_n^0(t) \equiv 2a_n^0(t)|_{He}$$

where $a_n^0(t)|_{He}$ are the inflow states from the Peters-He model[6]. Defining the inflow states with this factor of 2 will become more apparent in the coming sections. Based on the Peters-He theory, the relationship

between induced inflow states (α_n^m, β_n^m) and rotor pressure loading coefficients (τ_n^m) for an infinite number of blades is given by the following[5]:

$$(8) \qquad V \begin{bmatrix} \tilde{L}^{c^{-1}} & 0 \\ 0 & \tilde{L}^{s^{-1}} \end{bmatrix} \begin{Bmatrix} a_n^m \\ b_n^m \end{Bmatrix} = \frac{1}{2} \begin{Bmatrix} \tau^{rc} \\ \tau^{rs} \end{Bmatrix}$$

Where r is used as a harmonic number to distinguish row harmonics and column harmonics. Solving for the inflow states yields the following:

$$(9) \qquad \begin{Bmatrix} a_n^m \\ b_n^m \end{Bmatrix} = \frac{1}{2V} \begin{bmatrix} \tilde{L}^c & 0 \\ 0 & \tilde{L}^s \end{bmatrix} \begin{Bmatrix} \tau^{rc} \\ \tau^{rs} \end{Bmatrix}$$

However, for a rotor with a finite number of blades, the momentum equations are unsteady with blade passage and, hence, the inflow solutions are also unsteady. The momentum equations can be written in matrix form as follows:

$$(10) \qquad \begin{aligned} [M^c]\{\dot{\alpha}\} + V\left[\bar{L}^c\right]^{-1}\{\alpha\} &= \tfrac{1}{2}\{\tau^c\} \\ [M^s]\{\dot{\beta}\} + V\left[\bar{L}^s\right]^{-1}\{\beta\} &= \tfrac{1}{2}\{\tau^s\} \end{aligned}$$

where the mass matrices $[M]$ and the influence coefficient matrices $[\bar{L}]$ are closed form expressions from the Galerkin procedure. Also, note that the influence coefficient matrices are a modified form of the matrices found in the Peters-He model.

$$(11) \qquad [\bar{L}^c] = \begin{bmatrix} 2[I] & & & \\ & [I] & & \\ & & [I] & \\ & & & \ddots \end{bmatrix} [\tilde{L}^c]$$

which states that the zeroeth harmonic terms are doubled, all other terms remain unaffected. This will become more apparent in the following sections. However, $[\bar{L}^s] = [\tilde{L}^s]$ as in the Peters-He model.

Since the inflow distribution is considered unsteady with blade passage, a solution for the inflow includes a summation of harmonics. Also, due to the time derivative of the inflow states—which are comprised of sines and cosines—the solutions to the above differential equations are coupled and include terms of both $[M]$ and $[\bar{L}]$. The general solution is the sum of the steady and unsteady solutions. For the steady-state solution, the inflow states are Eq.(9) and the unsteady inflow solutions are

$$(12) \qquad \begin{Bmatrix} \{\alpha_n^m\}_c \\ \{\alpha_n^m\}_s \end{Bmatrix}_k = \frac{1}{2V}\left[\bar{\bar{L}}_k^c\right]\begin{Bmatrix} \{\tau_n^m\}_c \\ \{\tau_n^m\}_s \end{Bmatrix}_k$$

where, again, k takes on integer multiples of the number of blades. The matrices $[\bar{\bar{L}}]_k$ are defined below from the coupled momentum equations,

$$(13) \qquad \begin{aligned} \left[\bar{\bar{L}}^c\right]_k &= \begin{bmatrix} [\bar{L}^c]^{-1} & \frac{k}{V}[M^c] \\ -\frac{k}{V}[M^c] & [\bar{L}^c]^{-1} \end{bmatrix}^{-1} \\ &= \begin{bmatrix} [N^c]_k & -\frac{k}{V}[N^c]_k[M^c][\bar{L}^c] \\ \frac{k}{V}[\bar{L}^c][M^c][N^c]_k & [N^c]_k \end{bmatrix} \end{aligned}$$

where

$$(14) \qquad [N^c]_k \equiv \left[[\bar{L}^c]^{-1} + (\frac{k}{V})^2[M^c][\bar{L}^c][M^c]\right]^{-1}$$

Similar expressions exists for $[\bar{\bar{L}}^s]_k$ and likewise $[N^s]_k$.

Therefore, general solutions to the momentum equations (10) are the sum of all solutions—steady and unsteady—and are defined below.

$$(15) \qquad \begin{aligned} \{\alpha_n^m(t)\} &= \frac{1}{2V}[\bar{L}^c]\{\tau_n^{mc}\}_{0c} \\ &+ \sum_{k=Q_i}\left(\frac{1}{2V}[C]_k[\bar{L}^c]_k\{\tau_n^{mc}\}_k\right) \end{aligned}$$

where $[C]$ is the temporal tranformation matrix defined by the following:

$$(16) \qquad [C]_k \equiv \begin{bmatrix} \cos(kt) & 0 \\ 0 & \sin(kt) \end{bmatrix}$$

A similar expression exists for $\{\beta_n^m(t)\}$.

2.2. Swirl Correction

The matrix $[M]$ in Eq.(10) was originally derived from potential flow theory for an actuator disk. This implies that there is no angular momentum added to the flow through the disk and, consequently, no energy loss due to swirl. Makinen[2] showed that the effect of swirl could be accounted for in a rigorous manner in the context of a finite-state actuator disk by two adjustments: 1.) the induced flow at the rotor disk is taken to be parallel to the local rotor lift vector, 2.) the mass matrix is augmented to include the extra kinetic energy in the swirl velocity. The amount of added mass was found to be

$$(17) \quad [M^m]_{\tt swirl} = [M^m]\left[[I] + m\left(\frac{\kappa\lambda}{Q}\right)^2\left[[I]-[A^m]^2\right]^{-m}\right]$$

where m is the harmonic number for a given term, λ is the inflow ratio, Q is the number of blades, and κ is an empirical factor to account for the swirl velocity. Although κ is theoretically equal to 2.0, the best correlation with Goldstein was found for $\kappa = 2.2$. It should be noted that the apparent mass matrix takes the following form:

$$(18) \qquad [M^c] = \begin{bmatrix} [M^0] & & & \\ & [M^1] & & \\ & & \ddots & \\ & & & [M^m] \end{bmatrix}$$

where, $[M^0] = \frac{1}{2}[M^0]_{\tt He}$ is a modified form of the original mass matrix from the Peters-He model. A similar matrix exists for the sine representation ($[M^s]$) but with no zeroeth harmonic terms.

In the derivation of this swirl correction by Makinen, it was assumed (in the context of a helicopter) that λ is small such that $\lambda^2 \ll 1$. However, in order to correlate with Goldstein results, one must allow for λ to be of the order unity or larger. Therefore, it is necessary to extend the formula in Eq.(17) to large λ. This implies replacing $\kappa^2\lambda^2$ in this equation with a more general $f(\lambda)$. In order to do this, we ran our

numerical Goldstein solution for rotors with 2, 4, and 6 blades over climb ratios from 0 to 3.0. We then optimized the swirl correction function based on the most rapid convergence of the finite-state model to the induced power efficiency as found from the numerically exact Goldstein results.
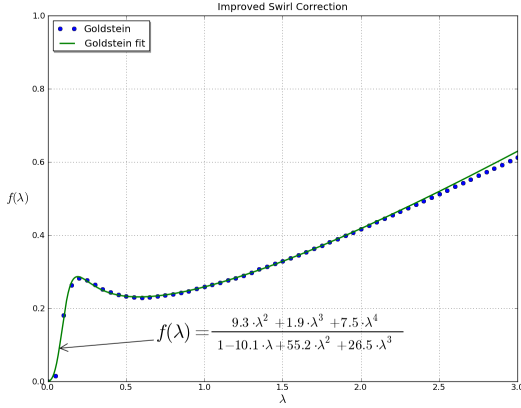

Figure 1: Function approximation to correct for swirl velocities in rotor wake.

Results for the optimum $f(\lambda)$ were found to be relatively insensitive to blade number so that a single expression could be found, as shown in Fig.1. The resulting curve was then fit with a rational polynomial in λ, also shown in the figure. At small λ, the new swirl correction behaves as $9.3\lambda^2$ ($\kappa \approx 3.0$) whereas the result in Makinen gave $\kappa = 2.2$ for the optimum fit. In revisiting the optimization results of Makinen, we discovered that the lower value of κ found in that work was due to the attempt of the optimizer to lower the error at larger values of λ. The new factor improves correlation at all inflow ratios. It should be noted that the efficiencies become very low for $\lambda > 1$ such that the "optimum" value is fitting a very small number. The important part of $f(\lambda)$ for practical considerations is for $\lambda < 0.5$ where the new formula is a significant improvement over that of Makinen. This new formula is used in all of the results to follow.

2.3. Induced Power

The starting point of this development is the computation of power based on finite-state variables. The induced power (i.e., the work done on the flow) of a rotor can be defined from fundamental physics. This is the time-average of the integration over the disk of the product of induced velocity, force per unit area, and unit area.

$$(19) \qquad C_P = \frac{1}{2\pi} \int\limits_0^{2\pi} \left(\iint\limits_A (\Delta P \cdot w)\, dA \right) d\bar{t}$$

where $w = w(r, \psi, t)$ is the induced velocity (Eq.(1)) and $P = P(r, \psi, t)$ is the force per unit area (Eq.(5)). Due to the orthogonality of the basis functions, the

above equation can be reduced to a more compact form.

$$(20) \qquad C_P = \frac{1}{2\pi} \int\limits_0^{2\pi} \{\tau\}^T \{\alpha\}\, d\bar{t}$$

where, for the sake of brevity, $\{\alpha\}$ represents the total inflow solution and likewise $\{\tau\}$ the total pressure expansion. From the inflow solutions in Eq.(15) and the pressure coefficients expanded in temporal harmonics—similar to Eq.(6)—the induced power coefficient is expressed as a summation as well.

$$(21) \qquad C_P = \{\tau^c\}_{0c}^T \{\alpha\}_{0c} + \frac{1}{2} \sum_k \left(\left\{ \begin{array}{c} \tau_k^c \\ \tau_k^s \end{array} \right\}^T \left\{ \begin{array}{c} \alpha_k \\ \beta_k \end{array} \right\} \right)$$

where, here, the sines and cosines have been averaged over the time-domain and the factor of 2 in Eq.(7) cancels the $\frac{1}{2}$ from the sinusoidal average, hence the reason for defining our inflow states with this factor of 2 earlier. Although a solution exists for the inflow states, this solution is in terms of the pressure expansion coefficients τ. Therefore, to determine the result to Eq.(21), knowledge of τ must be sought.

2.4. Blade-Element Theory

In order to represent the loadings $\{\tau\}$ and, hence, rotor power C_P in terms of some meaningful controls, we now apply blade-element theory. The lift per unit length per blade $\mathscr{L}_q$ is written in terms of standard airfoil theory with the lift coefficient $C_\mathscr{L}$ proportional to the sine of the angle of attack.

$$(22) \qquad C_\mathscr{L} = a \sin(aoa)$$

which is the exact result of 2-D potential flow theory. The velocity may then be written in terms of the tangential and perpendicular components of flow at the blade (as in standard rotorcraft notation),

$$(23) \qquad V^2 = U_T^2 + U_P^2$$

and the angle of attack is the pitch angle θ minus the inflow angle.

$$(24) \qquad aoa = \theta - \tan^{-1}\left(\frac{U_P}{U_T} \right)$$

The lift per unit length per blade then takes on the classic form in terms of U_T and U_P,

$$(25) \qquad \mathscr{L}_q(\theta) = \frac{1}{2}\varrho ac\left(U_T^2 \theta_q - U_T U_P \right)$$

where θ_q represents the pitch angle for each blade.

One may then express the pitch angle per blade as an expansion in harmonics of blade azimuthal pitch and blade radial twist.

$$(26) \qquad \theta_q \equiv \sum_{k,m} \left[\bar{r}^k \left[\theta_k^{mc} \cos(m\psi_q) + \theta_k^{ms} \sin(m\psi_q) \right] \right]$$

One may now determine the loadings on the rotor as an expression of the lift, which are given in terms of tip speed ΩR and nondimensional radial position $\bar{r}$.

$$(27) \qquad \left\{ \begin{array}{c} \tau_n^{0c} \\ \tau_n^{mc} \\ \tau_n^{ms} \end{array} \right\} = 2 \sum_{q=1}^Q \int_0^1 \mathscr{L}_q \phi_n^m(\nu) d\bar{r} \left\{ \begin{array}{c} \frac{1}{2} \\ \cos(m\psi_q) \\ \sin(m\psi_q) \end{array} \right\}$$

where

$$\bar{\mathscr{L}}_q = \frac{\mathscr{L}_q}{2\pi\varrho\Omega^2 R^3} \tag{28}$$

is the non-dimensional form of the lift per unit length per blade, Q is the total number of blades, and ϕ_n^m is defined as the following polynomial.

$$\phi_n^m(\nu) \equiv \frac{1}{\nu}\bar{P}_n^m(\nu) \tag{29}$$

If one defines the lift as an expansion in harmonics of Legendre functions, as was done with the pitch angle:

$$\bar{\mathscr{L}}_q \equiv \frac{\bar{r}}{Q}\sum_{m,n}\left(\gamma_n^{mc}\cos(m\psi_q) + \gamma_n^{ms}\sin(m\psi_q)\right)\bar{P}_n^m \tag{30}$$

then the blade loadings may be expressed in a very simplified form.

$$\left\{\begin{matrix} \tau_n^{0c} \\ \tau_n^{mc} \\ \tau_n^{ms} \end{matrix}\right\} = 2\sum_{q=1}^{Q}\int_0^1 \bar{\mathscr{L}}_q\bar{P}_n^m\frac{d\bar{r}}{\nu}\left\{\begin{matrix} \frac{1}{2} \\ \cos(m\psi_q) \\ \sin(m\psi_q) \end{matrix}\right\} \tag{31}$$

The above integral can be evaluated by substitution of the following matrix:

$$\left[E_{nj}^{mr}\right] \equiv \int_0^1 \bar{P}_n^m(\bar{r})\bar{P}_j^r(\bar{r})d\bar{r} \tag{32}$$

where

$$\left[E_{nj}^{mm}\right] = [\delta_{nj}] = [I] \tag{33}$$

This gives a closed form expression for the blade loadings.

$$\begin{aligned} \{\tau_n^{mc}\}_k &= [T^c]_k\{\gamma_j^{rc}\} \\ \{\tau_n^{ms}\}_k &= [T^s]_k\{\gamma_j^{rs}\} \end{aligned} \tag{34}$$

where the matrices $[T^c]$ and $[T^s]$ are defined from the orthogonality matrix Eq.(32)[1].

$$[T^c]_k \equiv \begin{bmatrix} [T^{cc}]_k & [0] \\ [0] & [T^{cs}]_k \end{bmatrix} \tag{35}$$

and

$$[T^s]_k \equiv \begin{bmatrix} [0] & [T^{ss}]_k \\ [T^{sc}]_k & [0] \end{bmatrix} \tag{36}$$

Here, the superscripts (i.e., cs) indicate if a zero harmonic term is included and the subscript k defines the allowed harmonics.

---

[1]See Appendix for more detailed explaination of $[T^x]$.

2.5. Rotor Loadings

General rotor performance theory encompasses rotor loads as well as induced power. Rotor loads in turn are also utilized as the constraints that define optimum induced power. The dynamic inflow formulation may be used to compute any desired rotor loads. Here we consider "rotor loads" to be integrals over the disk of the pressure including appropriate weighting functions. We will now express rotor loads in terms of the pressure loading coefficients $\{\tau\}$. Consider, for example, rotor thrust, roll moment, and pitching moment—three common rotor loads. These loads are defined by the following integrals of the pressure loading:

$$\begin{aligned} C_T &= \frac{1}{\pi}\int_0^{2\pi}\int_0^1 \Delta P\bar{r}d\bar{r}d\psi \\ C_M &= -\frac{1}{\pi}\int_0^{2\pi}\int_0^1 \bar{r}\Delta P\bar{r}d\bar{r}\cos(\psi)d\psi \\ C_L &= -\frac{1}{\pi}\int_0^{2\pi}\int_0^1 \bar{r}\Delta P\bar{r}d\bar{r}\sin(\psi)d\psi \end{aligned} \tag{37}$$

After substituting the pressure loading of the Peters-He theory from Eq.(5) and integrating, the rotor loads are readily expressible in closed-form. In terms of the pressure loadings—and written in matrix form—the rotor loads are:

$$\left\{\begin{matrix} C_T \\ C_M \\ C_L \end{matrix}\right\} = \begin{bmatrix} \frac{2}{\sqrt{3}} & 0 & 0 \\ 0 & -\sqrt{\frac{2}{15}} & 0 \\ 0 & 0 & -\sqrt{\frac{2}{15}} \end{bmatrix}\left\{\begin{matrix} \tau_1^{0c} \\ \tau_2^{1c} \\ \tau_2^{1s} \end{matrix}\right\} \tag{38}$$

This example may be extended to formulate any desired rotor loads. One may therefore write the general loading vector $\{C\}$ in the form:

$$\{C\} = [D]\{\tau\} \tag{39}$$

where $[D]$ is a closed-form matrix based on integrals of the inflow shape functions.

3. OPTIMIZATION

3.1. Optimum Power

With the solutions to the inflow states (Eq.(15)), and the expression for the loadings (Eq.(34)) substituted into Eq.(21), the result is the following:

$$C_P = \frac{1}{2V}\{\gamma\}^T[R]\{\gamma\} \tag{40}$$

where a definition has been made to simplify the expression. The matrix $[R]$ contains the influence coefficients which, for the case of finite number of blades, is a summation of harmonics of influence coefficients.

$$[R] \equiv [\bar{L}] + \sum_k\left([T^c]_k^T[\bar{\bar{L}}^c]_k[T^c]_k + [T^s]_k^T[\bar{\bar{L}}^s]_k[T^s]_k\right) \tag{41}$$

where,

$$[\bar{L}] = \begin{bmatrix} [\bar{L}^c] & [0] \\ [0] & [\bar{L}^s] \end{bmatrix} \tag{42}$$

Also, the loading vector has, for the sake of brevity, been simplified.

$$(43) \qquad \{\gamma\} = \left\{ \begin{array}{c} \{\gamma_n^{mc}\} \\ \{\gamma_n^{ms}\} \end{array} \right\}$$

The result in Eq.(40) can then be optimized under given constraints on $\{\tau\}$. One may scale the general loading vector from Eq.(39) against the thrust C_T.

$$(44) \qquad \{C\} = C_T \left\{ \begin{array}{c} 1 \\ c_m \\ c_l \end{array} \right\} \equiv [G]^T \{\gamma\}$$

where, here, we've defined a scaled pitch moment coefficient c_m and roll moment coefficient c_l. The matrix $[G]$ is comprised of the constraints on the loads which contains the previously defined matrices $[D]$ and $[T]$ from Eqs.(39) and (34), respectively.

Following the method used by Peters & File [7], one may now minimize the induced-power C_P subject to the constraints $\{\gamma\}^T[G]$. The result is a very compact formulation for the induced power.

$$(45) \qquad (C_P)_{opt} = \frac{C_T^2}{2V} \left\{ \begin{array}{c} 1 \\ c_m \\ c_l \end{array} \right\}^T \left[G^T R^{-1} G \right]^{-1} \left\{ \begin{array}{c} 1 \\ c_m \\ c_l \end{array} \right\}$$

$$\equiv \frac{C_T^2}{2V} \{\zeta\}^T [Q]^{-1} \{\zeta\}$$

where $\{\zeta\}$ is a vector of scaled constraints on the loads (e.g., thrust, roll moment, etc.) from Eq.(39) and the symmetric matrix $[Q]$ contains the effects due to controls (e.g., pitch angle θ, inflow skew angle χ, etc.) among other parameters as number of blades and swirl correction.

3.2. Induced Power Efficiency

It is known from Glauert [8] that the minimum possible power is given by

$$(46) \qquad (C_P)_{ideal} = \frac{C_T^2}{2V}$$

One can normalize the above relation by dividing both sides by C_T^2.

$$(47) \qquad \left(\frac{C_P}{C_T^2} \right)_{ideal} = \frac{1}{2V}$$

This is the classic Glauert minimum.

We may define the Induced Power Efficiency (ε_{IP}) as the ratio of the minimum Glauert induced power divided by the optimum power (for a constrained case above). The optimum power can then be divided by C_T^2 to obtain a formula for computing this power with the scaled constraints.

$$(48) \qquad \left(\frac{C_P}{C_T^2} \right)_{opt} = \frac{1}{2V} \{\zeta\}^T [Q]^{-1} \{\zeta\}$$

One may then take a ratio of the Glauert minimum to the optimum power (with constraints on the available controls and loads) to get the ε_{IP}.

$$(49) \qquad \varepsilon_{IP} = \frac{(C_P/C_T^2)_{ideal}}{(C_P/C_T^2)_{opt}} = (\{\zeta\}^T [Q]^{-1} \{\zeta\})^{-1}$$

The induced power efficiency ε_{IP} is always a number between 0 and 1. The vector $\{\zeta\}$ and each of the matrices in $[Q]$ represents the effect of a given physical variable on the induced power efficiency. It may be noted that the ε_{IP} is analogous to the Figure of Merit used as a measure of efficiency of a rotor in the hover condition.

4. RESULTS

Figure 2 shows results with and without the effect of lift tilt (i.e., swirl velocities). This is possible because the effect of blade number is distinct from the effect of swirl. Cases are run for 2, 4, and 6 blades. Note that, at larger values of V_∞, the effect of swirl dominates, whereas at lower climb rates the effect of blade number becomes dominate.
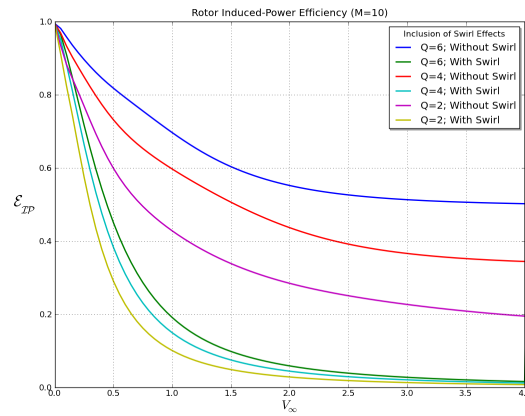

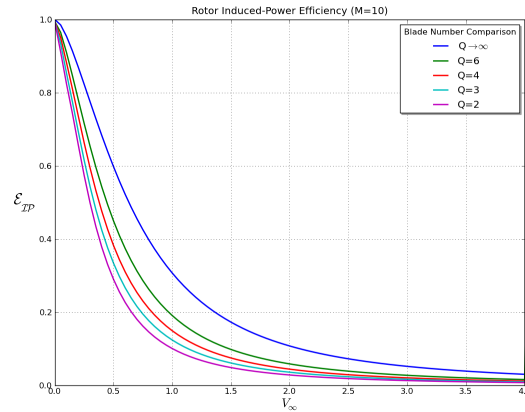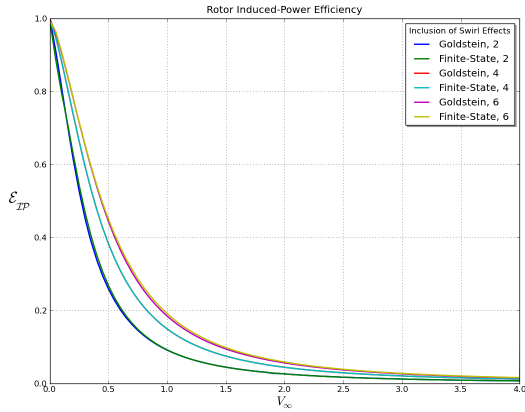Figure 2: The effects of swirl due to inclination of the lift vector.

Figure 3: Increasing the number of blades increases the rotor induced-power efficiency.
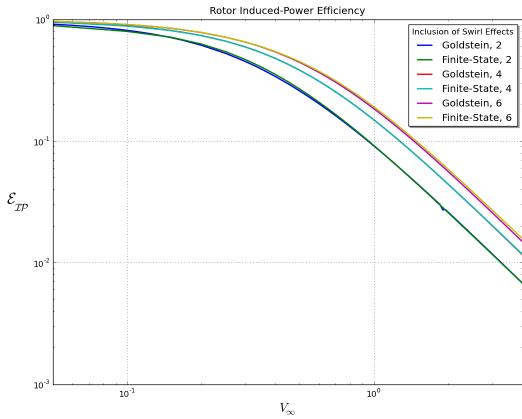
Figure 3 gives induced power efficiency as a function of V_∞ which—for axial flow—is identical to the non-dimensional climb rate λ and the mass-flow parameter V. Curves are shown for an infinite number of blades (which is the Glauert momentum optimum) and also for $Q = 2, 3, 4$, and 6. The limit to this finite blade number

efficiency—provided by Betz[9]—states that the minimum power is achieved when the trailing vortex sheet is contained along a helical path behind the rotor. One can see the clear effect of blade number on efficiency. For this optimization, $M = 12$ is virtually full control authority on available blade twist.

Figure 4 shows that increasing the available harmonics drives the convergence towards that of Goldstein. The data in Fig.4(b) was plotted on a logarithmic scale to accentuate the high order of agreement. From these graphs one can see that the finite-state method converges to the Goldstein results at all blade numbers.
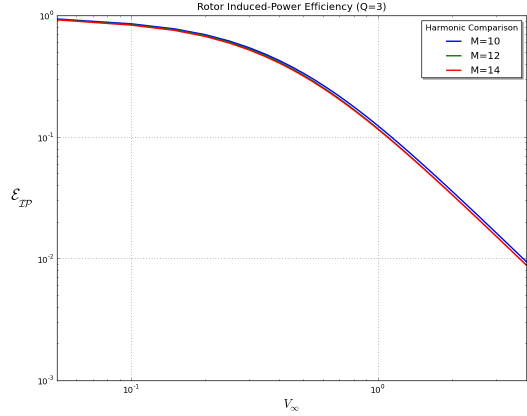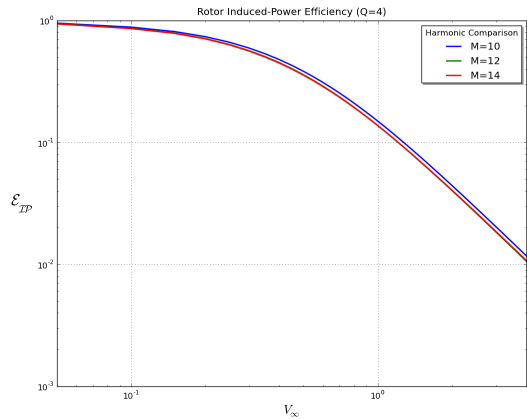

(a) Harmonic comparisons with 3 blades.

(a) Plot for $Q = 2, 4, 6$.

(b) Harmonic comparisons with 4 blades.

(b) Logarithmic plot for $Q = 2, 4, 6$.

(c) Harmonic comparisons with 6 blades.

Figure 4: Rapid convergence to the solutions of Goldstein by the Finite-State method.

Figure 5: Finite-state iteration—as number of harmonics is increased—indicates that 12 harmonics is sufficient for convergence.
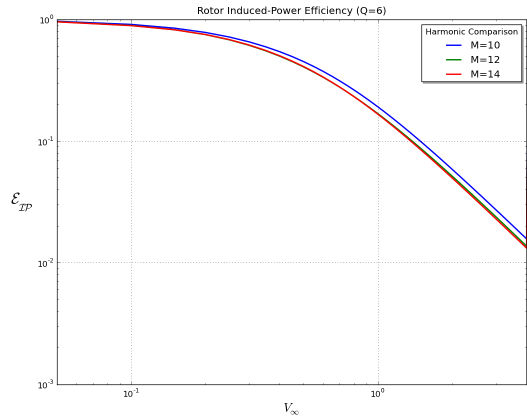
Figure 5 shows that a reduction in the degrees of freedom for blade twist does not have a large effect on efficiency as long as there is enough freedom to change the linear twist. One can see also the rapid convergence towards that of Goldstein by increasing the number of allowed harmonics. Here a solution that includes only 12 harmonics is quite sufficient to agree with the results from Goldstein.

5. CONCLUSION

Applying the finite-state model to the dynamic inflow of the lifting rotor proves viable to a working solution of the induced-power for rotors with finite blade number. This formulation applies blade-element theory to account for the rotor loads on each blade. Combining these two theories has rendered an improved correction

factor over the previous quadratic function to account for the swirl velocities in the rotor wake.

The modified correction factor has provided greater insight to the nature of the swirl velocities that had previously remained obscure. The presence of swirl vortices dramatically increases the induced-power demand and, thus, decreases the performance of the rotor for a given number of blades. However, the previous quadratic term drives the inflow solution to diverge from the results of Goldstein at inflow ratios close to unity. The improved swirl function compensates for the unique behavior at these higher velocities.

Blade number has a direct effect on the induced-power efficiency of the helicopter rotor. By introducing higher blade numbers, the rotor then redistributes the load throughout the disk in a more efficient manner—thus, increasing the number of blades increases the efficiency of the induced-power of the rotor.

The results presented were found to be in close agreement with previous investigations by Goldstein and others of induced power of the lifting rotor operating at moderate to high inflow ratios. Insights from this investigation should help to guide the design of future high-speed rotorcraft with higher aerodynamic efficiency.

APPENDIX

$[T_k^{xx}]$ Matrix

The orthogonality matrix $[E_{nj}^{mr}]$ defined in Eq.(32) follows the notation from the Peters-He inflow theory. From the definition of the orthogonality matrix, the pressure loading coefficients may be expressed in the following manner:

(A-1) $\quad \{\tau_n^{0c}\} = \sum_{r,j} E_{nj}^{0r} \left(\gamma_j^{rc} \cos(rt) + \gamma_j^{rs} \sin(rt) \right)$

$$\{\tau_n^{mc}\} = \sum_{r,j} E_{nj}^{mr} \left[\gamma_j^{rc} \left(\cos\left((m+r)t\right) + \cos\left((m-r)t\right) \right) \right.$$
$$\left. + \gamma_j^{rs} \left(\sin\left((m+r)t\right) - \sin\left((m-r)t\right) \right) \right]$$

$$\{\tau_n^{ms}\} = \sum_{r,j} E_{nj}^{mr} \left[\gamma_j^{rc} \left(\sin\left((m+r)t\right) + \sin\left((m-r)t\right) \right) \right.$$
$$\left. - \gamma_j^{rs} \left(\cos\left((m+r)t\right) - \cos\left((m-r)t\right) \right) \right]$$

The above equations may be recast into a set of matrices that map the lift coefficients γ_j^r to the pressure expansion coefficients τ_n^m for a given blade harmonic k. These matrices are partitioned by the sum/difference of m and r based on the following:

(A-2) $\qquad\qquad |m \pm r| = k$

which comes about from the use of trigonometric rules when carrying out the integrals in Eq.(31). The above relation states the only values that are allowed in the computation are the sum and/or difference of harmonic numbers that are, in turn, equal to integer multiples of blade number (i.e., $k = 0, Q, 2Q, \cdots$). This, along with the orthogonality of the Legendre functions, allows values from Eq.(32) into only partitions of m and r that are equal to k, Eq.(A-2). All other harmonic partitions are zero.

This defines a simple set of matrices that may be used to transform the influence coefficient matrices into the appropriate harmonics for a rotor with a given number of blades.

To demonstrate this assume a rotor with, say, 2 blades. Then, the only allowable blade harmonics are $k = 0, 2, 4, 6, \cdots$ up to a maximum harmonic k_{max}. To illustrate further, below are the matrix partitions for the example of $k = 2$:

$[T_2^{cc}] \Rightarrow$

$m \backslash r$	0	1	2	3	4
0			E^{02}		
1		E^{11}		E^{13}	
2	$2E^{20}$				$\ddots$
3		E^{31}			
4			E^{42}		
5				$\ddots$	

$[T_2^{cs}] \Rightarrow$

$m \backslash r$	1	2	3	4	5
0		E^{02}			
1	E^{11}		E^{13}		
2				E^{24}	
3	$-E^{31}$				$\ddots$
4		$-E^{42}$			
5			$\ddots$		

$[T_2^{sc}] \Rightarrow$

$m \backslash r$	0	1	2	3	4
1		E^{11}		$-E^{13}$	
2	$2E^{20}$				$\ddots$
3		E^{31}			
4			E^{42}		
5				$\ddots$	

$[T_2^{ss}] \Rightarrow$

$m \backslash r$	1	2	3	4	5
1	$-E^{11}$		E^{13}		
2				E^{24}	
3	E^{31}				$\ddots$
4		E^{42}			
5			$\ddots$		

where the submatrix, say, E^{31} takes the following form:

(A-3) $\qquad [E_{n,j}^{3,1}] = \int_0^1 \bar{P}_n^3(\nu) \bar{P}_j^1(\nu) d\nu$

The partitions of the harmonic transformation matrix $[T_k^{xx}]$ where $|m \pm r| \neq k$ are zero matrices.

The above relations therefore reduce the pressure integrals of Eq.(31) to the compact matrix representation found in Eq.(34)

References

[1] Goldstein, S., "On the Vortex Theory of Screw Propellers," Proceedings of the Royal Society of London. Series A, Containing Papers of a Mathematical and Physical Character, Vol. 123, The Royal Society, April 6, 1929, pp. 440-465.

[2] Makinen, Stephen M., *Applying Dynamic Wake Models to Large Swirl Velocities for Optimal Propellers*, Doctor of Science Thesis, Washington University in St. Louis, May 2005.

[3] Garcia-Duffy, Cristina, *Applying Dynamic-Wake Models to Induced Power Calculations for an Optimum Rotor*, Ph.D. thesis, Washington University, December 2008.

[4] Modarres, Ramin and Peters, David A., "Efficient Solution of Goldstein's Equations for Propellers With Application to Rotor Induced Power Efficiency," Proceedings of the 38th European Rotorcraft Forum, Amsterdam, Sept. 4-7, 2012.

[5] Peters, David A. and He, Cheng Jian, "Correlation of Measured Induced Velocities with a Finite-State Wake Model," *Journal of the American Helicopter Society*, Vol. 36, No. 3, July 1991, pp. 59-70.

[6] He, Cheng Jian, *Development and Applications of a Generalized Dynamic Wake Theory for Lifting Rotors*, Ph.D. Dissertation, Georgia Institute of Technology, August 1989.

[7] Peters, David A., File, Chad L., Ormiston, Robert A., "Rotor Performance and Optimum Power from Finite-State Inflow with Realistic Constraints," Proceedings of the AHS International 67th Annual Forum and Technology Display, Virginia Beach, VA, May 3-5, 2011.

[8] Glauert, H., "A General Theory of the Autogyro," R&M No. 1111, Aeronautical Research Council of Great Britain, March 1927.

[9] Betz. A. and Prandtl, L., "Schraubenpropeller mit geringstem energieverlust," Goettinger Nachrichten, March 1919, pp. 193-217.